NUMERICAL STUDIES OF BODY WAVE AMPLITUDES IN FULL WAVEFORM ACOUSTIC LOGS

by

Zhang Jinzhong* and C.H. Cheng

Earth Resources Laboratory
Department of Earth, Atmospheric, and Planetary Sciences
Massachusetts Institute of Technology
Cambridge, MA 02139

ABSTRACT

The amplitudes of P and S head waves in a full waveform acoustic log microseismogram are studied numerically as a function of borehole and formation parameters. The technique used is contour integration around the respective branch cuts in the complex wavenumber plane (Tsang and Rader, 1979). The results showed that the P wave amplitude depends on the Poisson's ratio, but the S wave amplitude does not. The well accepted geometric spreading factor for P and S waves in the "far field" is only valid for a limited range of source-receiver spacings, and the onset of "far field" depends on the Poisson's ratio as well as the wavelength. The wave shape factor I_c for the P wave as defined by Lebreton *et al.* (1978) has a direct relationship to *in situ* attenuation.

INTRODUCTION

Synthetic microseismograms are extremely useful tools for studying the behavior of full waveform acoustic logs in different borehole environments. It allows us to investigate the arrivals and amplitudes of different body waves and guided waves, and how they are affected by formation velocities, attenuation, borehole radius and fluid (mud) properties. However, most of the studies so far have concentrated on the generation of the total waveform using different forms of the real axis integration technique. This technique is rather time consuming and does not allow for the separation of different arrivals. In order to isolate the formation and borehole effects on the different body and guided waves, it is necessary to generate the different waves separately. Tsang and Rader (1979) used contour integrals to study the effects of formation velocity on the P and S wave amplitudes. Kurkjian (1983) discussed the separation of the S wave from the pseudo-Rayleigh wave in the complex wavenumber domain. In both papers, only the elastic case (no attenuation) was considered.

---

*Permanent address: Xian Institute of Petroleum, Xian, People's Republic of China.

In this paper, we will present a complete study of the dependence of body wave amplitudes on different formation parameters such as formation velocities and attenuation, Poisson's ratio, frequency (and by inference borehole radius), fluid velocity and source-receiver separation. The technique used is the contour integration technique of Tsang and Rader (1979). Attenuation is introduced by the use of complex velocities (Cheng *et al.*, 1982). By such a study, we hope to gain some insight into the dependence of the body wave amplitudes on these various parameters. This knowledge is crucial in the measurement of *in situ* attenuation as well as in the developing area of full waveform inversion.

THEORETICAL BACKGROUND

The pressure response $P(r,z,t)$ in a fluid-filled borehole at an axial distance z and radial distance r from a point isotropic source is well known (Tsang and Rader, 1979; Cheng *et al.*, 1982). It is given by

$$P(r,z,t) = \int_{-\infty}^{\infty} S(\omega)\, e^{-i\omega t} \int_{-\infty}^{\infty} [K_0(fr) + GI_0(fr)]\, e^{ikz}\, dk, \tag{1}$$

where $S(\omega)$ is the Fourier spectrum of the source. G is given by

$$G = \frac{gK_1(fR) - K_0(fR)}{gI_1(fR) + I_0(fR)} \tag{2}$$

and

$$g = \frac{f\rho}{l\rho_f}\left\{\left(\frac{2\beta^2}{c^2} - 1\right)^2 \frac{K_0(lR)}{K_1(lR)} - \frac{2\beta^2 lm}{\omega^2}\left[\frac{1}{mR} + \frac{2\beta^2}{c^2}\frac{K_0(mR)}{K_1(mR)}\right]\right\} \tag{3}$$

where

$$l = k\left(1 - \frac{c^2}{\alpha^2}\right)^{1/2} = \omega\left(\frac{1}{c^2} - \frac{1}{\alpha^2}\right)^{1/2};$$

$$m = k\left(1 - \frac{c^2}{\beta^2}\right)^{1/2} = \omega\left(\frac{1}{c^2} - \frac{1}{\beta^2}\right)^{1/2};$$

$$f = k\left(1 - \frac{c^2}{\alpha_f^2}\right)^{1/2} = \omega\left(\frac{1}{c^2} - \frac{1}{\alpha_f^2}\right)^{1/2};$$

ω is the angular frequency; c is the phase velocity; $k = \omega/c$ is the axial wave number; α, β, and α_f are the P and S wave velocity of the formation and the borehole fluid velocity, respectively; R is the borehole radius; ρ and ρ_f are the formation and fluid density; and I_i and K_i are the modified Bessel functions of the i^{th} order. The $K_0(fr)$ term in the k integral represents the source term and the $GI_0(fr)$ term represents the response of the borehole.

To generate the complete microseismogram, one needs to integrate along the real k axis. However, in this paper, we are interested only in the contributions of the P and S head waves. These contributions can be obtained by evaluating the integral along the respective branch cuts (Tsang and Rader, 1979). In particular, for the P head wave, we choose a branch cut in the first quadrant of the complex k plane along the line

$$\mathrm{Re}\, k = \frac{\omega}{\alpha},$$

and for the S head wave, along the line

$$\mathrm{Re}\, k = \frac{\omega}{\beta}.$$

With these choices of the branch cuts, the source term is analytic across both of the cuts and can be ignored. We need only to examine the response term in Eq. 1. Details of the integration path can be found in Tsang and Rader (1979).

The effect of formation and fluid attenuation can be introduced through the use of complex velocities. The transformation is:

$$v(\omega) = v(\omega_0)\left[1 + \frac{\ln(\omega/\omega_0)}{\pi Q}\right](1 + i/2Q)^{-1}. \tag{4}$$

where $v(\omega)$ is the modified formation or fluid body wave velocity, $v(\omega_0)$ the corresponding velocity at the reference frequency ω_0, and Q the quality factor for that body wave.

The source-time function used in this study is the modified Tsang and Rader source described in the Appendix of Toksöz *et al.* (1983).

RESULTS AND DISCUSSIONS

Using the contour integration discussed in Tsang and Rader (1979) and the branch cuts given above, we can study the variations in the P and S wave amplitudes in full waveform acoustic logging microseismograms as a function of borehole, formation and tool parameters. In particular, we will examine the effects of formation Poisson's ratio, the critical incident angle (a function of the fluid to formation velocity ratio), borehole radius (by extension source frequency), formation and fluid attenuation, and source-receiver separation on the head wave amplitudes. In general, we will be discussing the second peak amplitude of the first cycle of the head wave in the time domain (called E_2 by Tsang and Rader, 1979). In addition, in some cases we will also present the peak amplitude in the frequency spectrum. In the latter instance, we will refer to the amplitude as the Fourier amplitude.

Poisson's Ratio

We first study the effect of formation Poisson's ratio on the amplitudes. It has been reported (Tsang and Rader, 1979; Cheng and Toksöz, 1981) that the P

wave amplitude increases as the Poisson's ratio increases. Figure 1 shows the P wave amplitudes of three cases as a function of the Poisson's ratio. In all three cases, the variation in Poisson's ratio is obtained by varying the formation S wave velocity. The parameters used that are common to all three cases are: α = 3.5 km/s, α_f = 1.8 km/s, R = 10 cm, f = 10 kHz, ρ = 2.25 g/cm^3, ρ_f = 1.2 g/cm^3. Curve 1 is for a source-receiver spacing z = 1.5 m, without attenuation; curve 2 is the same but with Q_α = 100; and curve 3 is for z = 10 m without attenuation. It can been seen that the P wave amplitude depends strongly on the Poisson's ratio, and that this effect is as strong as, or maybe even stronger than that from a reasonable amount of attenuation. This effect decreases with increasing source-receiver spacing because of the geometric spreading factor for the P head wave.

In Figure 2, we have plotted the P wave amplitudes versus Poisson's ratios for a P wave velocity of α = 5.5 km/s. The rest of the parameters are the same as in curve 1 of Figure 1. Although the absolute amplitude of the P wave has decreased compared to Figure 1, the relative effects of the Poisson's ratio have remained similar.

In contrast to the P wave, the S wave shows no dependence on the formation Poisson's ratio (figure not shown), as long as the formation S wave and fluid velocities are held constant. This result confirms the conclusions of Cheng and Toksöz (1981) obtained by examining the entire microseismogram.

Critical Incident Angle

Comparing Figures 1 and 2, we see that for the same Poisson's ratio, the P wave amplitude decreases as the P wave velocity increases, with the fluid velocity remaining constant. This implies that the P wave amplitude increases with increasing fluid to P wave velocity ratio, or equivalently, as the critical incident angle from the fluid to the formation, $\vartheta_{ac} = \sin^{-1}(\alpha_f/\alpha)$, increases. This is shown in Figure 3 where the P wave amplitude is plotted as a function of the critical incident angle. The formation velocities are held at α = 5.5 km/s and β = 3.4 km/s with varying fluid velocity. The rest of the parameters are the same as in Figure 2. As can be seen in the figure, the P wave amplitude increases significantly with increasing ϑ_{ac}.

In Figure 4, we plotted the S wave amplitude as a function of the S wave incident angle $\vartheta_{\beta c} = \sin^{-1}(\alpha_f/\beta)$ as the formation velocities are held constant at α = 3.5 km/s and β = 1.94 km/s. The S wave amplitude also increases as a function of the increasing critical incident angle, but the increase is less than the corresponding P wave.

The changes in the P wave amplitude as a function of the critical incident angle can be understood in terms of the coupling of the particle motion from the fluid to the solid. For a small critical incident angle, the motion of the wave in the fluid is mainly in the radial direction, whereas the P head wave has a motion in the axial direction. Hence the couple is not efficient. This coupling improves as the incident angle increases and the particle motion in the fluid acquires a larger and larger axial component.

The changes in the S wave amplitude with incident angle cannot be understood in these simple terms, since the particle motion of the S head wave

is radial. However, as pointed out by Kurkjian (1983) and also shown later in this paper, the isolation of the S wave branch point is often complicated by the neighboring pseudo-Rayleigh wave pole. The changes in the S wave amplitude observed here may be due to the influence of the pseudo-Rayleigh wave. Further studies are needed before definitive conclusions can be drawn on the variations of the S wave amplitude with the critical incident angle.

Borehole Radius and Source Frequency

In Figure 5 we have plotted the P and S wave amplitude as a function of borehole radius with and without attenuation. The formation parameters are $\alpha = 3.5\ km/s$, $\beta = 1.94\ km/s$, $f_0 = 10\ kHz$ and $z = 1.5\ m$, and in the cases with attenuation, $Q_\alpha = 100$ and $Q_\beta = 60$. We can see that both the P and S wave amplitudes increase with increasing borehole radius. In the case for the P waves, this is consistent with the results of Tsang and Rader (1979) which showed increasing P wave amplitude with frequency. Since the propagation characteristics of any wave in a borehole are actually a function of kR, the product of the wavenumber and the radius, an increase in frequency is identical to an increase in borehole radius.

Our results for the S wave, however, are different from those shown in Tsang and Rader (1979). Specifically, they show a functional dependence of the S wave amplitude with frequency that has a peak at about 10 to 15 kHz, depending on formation parameters. We failed to observe this peak. One possible explanation is that the S wave amplitude calculated by the branch cut method is actually a combination of the S and pseudo-Rayleigh waves (Tsang and Rader, 1979). It is well known that the pseudo-Rayleigh wave amplitude has a peak as a function of frequency. The peak shown in Tsang and Rader is consistent with the peak in the spectrum for the first mode of the pseudo-Rayleigh wave. Our results are for the second peak amplitude in the time series, whereas the results of Tsang and Rader are Fourier amplitudes. As we can see later in this paper, these two amplitudes are not necessarily similar for the S wave, owing to the effect of the pseudo-Rayleigh wave.

Geometric Spreading Factor for P waves

One of the most important reasons for the study of head wave amplitudes is the determination of *in situ* attenuation. The variations of the head wave amplitude as a function of source-receiver separations under changing borehole and formation parameters are critical to the design of attenuation determination algorithms. Various authors (e.g. Winbow, 1980) have suggested that the P wave amplitude decreases linearly with source-receiver separation for an isotropic point source in the "far field." In order to quantify this statement, we have generated synthetic microseismograms for the P wave as a function of the source-receiver separation z in a variety of borehole and formation conditions. In the following figures, we have plotted our results for the P wave second peak (A_a) and Fourier (A'_a) amplitudes, both multiplied by the source-receiver separation z, as a function of z. In this way, we can clearly see the range of the validity of the assumption that the geometric spreading is proportional to $1/z$. Furthermore, we have defined the range of validity as that range in source-receiver separation within which the product of the amplitude and z changes by less than one percent from its peak value.

In Figure 6, we have plotted the P wave amplitude versus z for the formation parameters given in Figure 1. With this choice of parameters, the wavelength of the P wave λ_α is about 0.35 m. We can see from the figure that both $A_\alpha z$ and $A'_\alpha z$ increase with z to about 5 m and then slowly decrease. The range of validity is about 4 to 10 m. As seen in the following figures, this functional dependence on z is characteristic. The decrease at large z can be attributed to the higher order terms in $1/z$ which have been neglected in the previous analyses.

Figure 7 shows P wave amplitudes versus z for the same formation and borehole velocities in a borehole with a radius R = 15 cm. There is no significant difference between this figure and Figure 6, except that the range of validity for A'_α has been reduced slightly. So we can see that the borehole radius has little effect on the geometric spreading factor, as expected.

Returning to a borehole radius of R = 10 cm, we change the source frequency to f = 15 kHz, giving a wavelength of λ_α = 0.233 m. The results are shown in Figure 8. It is clear that the range of validity has been reduced and the $1/z$ geometric factor holds within the range of about 2 to 5 m.

In Figure 9, we have decreased the frequency to 5 kHz, giving a λ_α of 0.7 m. In this case, the range of validity is from about 7 m and beyond.

In Figure 10, we changed the formation velocities to α = 5.5 km/s, β = 3.05 km/s, maintaining a constant Poisson's ratio, and at a frequency of 10 kHz, to arrive at a wavelength of 0.55 m. The range of validity now is from 5 m outwards. Shortening the wavelength by increasing f to 15 kHz has the expected effect of decreasing the range of validity (Figure 11).

It was shown previously in this paper that the Poisson's ratio has a dramatic effect on the P wave amplitude. It is thus of great interest to investigate the effect of Poisson's ratio on the geometric spreading factor. In Figures 12 and 13 we have taken the model used in Figure 10 and varied the Poisson's ratio by changing the S wave velocity. Thus the P wave wavelength is kept constant. Figure 12 shows a case with Poisson's ratio σ = 0.33. As we can see, the range at which the $1/z$ geometric spreading assumption is valid is reduced to $3 < z < 5m$, significantly different from the case in Figure 10, without any changes in λ_α. In Figure 13, we have σ = 0.23, and again the range of validity is drastically altered. In this case, the $1/z$ assumption is not valid until a distance of about 10 meters. Thus we can see that the Poisson's ratio of the formation significantly affects the geometric spreading factor for the P waves.

Summarizing the results of this section, we can say that both the Poisson's ratio and the wavelength have a strong effect on the geometric spreading factor of the P wave. For a relatively low Poisson's ratio, σ = 0.23, typical of harder rocks (e.g. limestones), "far field" can be thought of as about 20 wavelengths from the source. For a medium Poisson's ratio, σ = 0.28, typical of high porosity sandstones, "far field" is about 10 wavelengths from the source. For a high Poisson's ratio, σ = 0.33, typical of soft sediments and shales, "far field" can be as near as 5 wavelengths away from the source. These are preliminary estimates from our numerical studies. A more extensive study is necessary to fully quantify these results. Nevertheless, it is clear that in order to obtain

correct *in situ* attenuation from the P waveform in field data, especially in the peak spectral amplitude method suggested by Cheng *et al.* (1982), the proper geometric spreading factor must be taken into account. A full waveform inversion will properly take this into consideration.

Geometric Spreading Factor for S waves

In the following section, we will present the results of our study of the S wave amplitudes as a function of source-receiver separation. Again, we will present both the second peak (A_β) and Fourier (A'_β) amplitudes. For an isotropic point source, Winbow (1980) has pointed out that the "far field" geometric spreading factor is proportional to $1/z^2$. Thus in presenting our results, we will be plotting the product of the amplitude and the square of the source-receiver separation ($A_\beta z^2$) versus z. Once again, we can define the range of validity of the geometric spreading factor as in the case for the P waves.

In Figure 14 we have plotted the S wave amplitudes versus distance for the same model used in Figure 6. In this case, the wavelength λ_β for the S wave is 0.194 m. As we can see from the figure, the $1/z^2$ geometric spreading factor assumption holds well for both A_β and A'_β from about 3 m outwards. However, in the case of the second peak amplitude, the $1/z^2$ assumption begins to break down beyond about 6 m. Once again, we can attribute this breakdown to the errors in the $1/z^2$ geometric factor.

Figure 15 shows the effect of the borehole radius. The borehole radius was decreased to R = 7.5 cm. All the rest of the parameters remained the same as in Figure 14. It can be seen that, similar to the P wave case, the borehole radius has little effect on the range of validity of the geometric spreading factor for the Fourier amplitude and has a small effect for the second peak amplitude.

In Figure 16 we changed the Poisson's ratio by changing the P wave velocity α to 3.1 km/s, giving a Poisson's ratio σ = 0.18. As we can expect from our studies in a previous section, the Poisson's ratio has virtually no effect on the amplitude of S waves.

Figure 17 shows the effect of the frequency and hence wavelength on the S wave geometric spreading factor. The source frequency is 7.5 instead of 10 kHz. λ_β is now 0.259 m. As expected, the range of validity shifts toward larger z, implying that the wavelength is one of the controlling factors in the onset of "far field".

Finally, we studied the dependence of the spreading factor on the S wave velocity. Formation velocities are changed to α = 5.5 km/s and β = 3.0 km/s with other parameters held constant. The results are plotted in Figure 18. The result for the second peak amplitude is similar to previous results, while for the Fourier amplitude, there does not appear to be a range for which the $1/z^2$ assumption is valid. Our interpretation of the results is that for the Fourier amplitude, since the cutoff for the pseudo-Rayleigh wave is lower for this model, its influence is larger. Once again, more detailed study is necessary to fully quantify this phenomenon.

The conclusion for this section is that the geometric spreading factor for the S wave is mainly controlled by its wavelength, with the Poisson's ratio and the borehole radius having little effect. However, the influence of the pseudo-Rayleigh wave must be taken into account.

Effect of Attenuation on P Wave Shape

It has been reported that the shape of the P wave in full waveform acoustic logs can be related to *in situ* permeability (Lebreton *et al.*, 1978). One explanation is that the attenuation of a porous rock is directly related to its permeability (Biot, 1956), and it is the dispersion caused by attenuation that gives rise to the change in wave shape. In this section we investigate the relationship between the shape of the P wave and the formation P wave attenuation. Following Lebreton *et al.* (1978), we defined the wave shape index I_c as follows:

$$I_c = \frac{A_2 + A_3}{A_1}, \tag{5}$$

where A_i are the absolute amplitudes of the i^{th} peaks (positive or negative) of the P wave. Figure 19 shows a plot of I_c versus Q_α^{-1}. We can see that there is an approximate linear relationship between I_c and Q_α^{-1}. Thus I_c is indeed a good measure of *in situ* attenuation, and through the model for a porous rock, the *in situ* permeability.

CONCLUSIONS

In this paper we have studied the variations of P and S wave amplitudes with formation and borehole parameters using the technique of contour integration (Tsang and Rader, 1979). The results of this study can be summarized as follows:

(1) Formation Poisson's ratio has a strong effect on the P wave amplitude but little or no effect on the S wave amplitude.

(2) Both the P and S wave amplitudes increase with increasing critical incident angle.

(3) Both the P and S wave amplitudes increase with increasing borehole radius. However, the S wave amplitude is influenced by the pseudo-Rayleigh wave when the cutoff frequency of the latter is brought below the source frequency by the increasing borehole radius.

(4) Within a certain range of source-receiver spacing, the P wave amplitude has a geometric spreading factor of $1/z$, while the S wave amplitude has a geometric spreading factor of $1/z^2$, as suggested previously by different authors. This range is a function of the wavelength of the P and S waves. However, this range for the P wave changes strongly with the Poisson's ratio.

(5) The wave shape factor for the *P* wave varies linearly with *in situ* attenuation.

ACKNOWLEDGEMENTS

This research is supported by the Full Waveform Acoustic Logging Consortium at M.I.T.

REFERENCES

Biot, M.A., 1956, Theory of propagation of elastic waves in a fluid-saturated porous rock: I. Low frequency range: J. Acous. Soc. Am., v.28, p.168-178.

Cheng, C.H. and Toksöz, M.N., 1981, Elastic wave propagation in a fluid-filled borehole and synthetic acoustic logs: Geophysics, v.46, p.1042-1053.

Cheng, C.H., Toksöz, M.N., and Willis, M.E., 1982, Determination of in situ attenuation from full waveform acoustic logs: J. Geophys. Res., 87, 5477-5484.

Kurkjian, A.L., 1983, Farfield decomposition of acoustic waveforms in a fluid-filled borehole: J. Acous. Soc. Am., v.74, supp.1, p.s88.

Lebreton, F., Sarda, J.P., Trocqueme, F., and Molier, P., 1978, Logging tests in porous media to evaluate the influence of their permeability on acoustic waveforms: Trans. 19th SPWLA Ann. Logging Symp., Paper Q.

Toksöz, M.N., Cheng, C.H., and Willis, M.E., 1983. Seismic waves in a borehole— a review: M.I.T. Full Waveform Acoustic Logging Consortium Annual Report, Paper 1.

Tsang, L. and Rader, D., 1979, Numerical evaluation of the transient acoustic waveform due to a point source in a fluid-filled borehole: Geophysics, v.44, p.1706-1720.

Winbow, G.A., 1980, How to separate compressional and shear arrivals in a sonic log: presented at the 50th Ann. Int. Meeting of Soc. Expl. Geophys., Houston, Texas, Nov. 16-20.

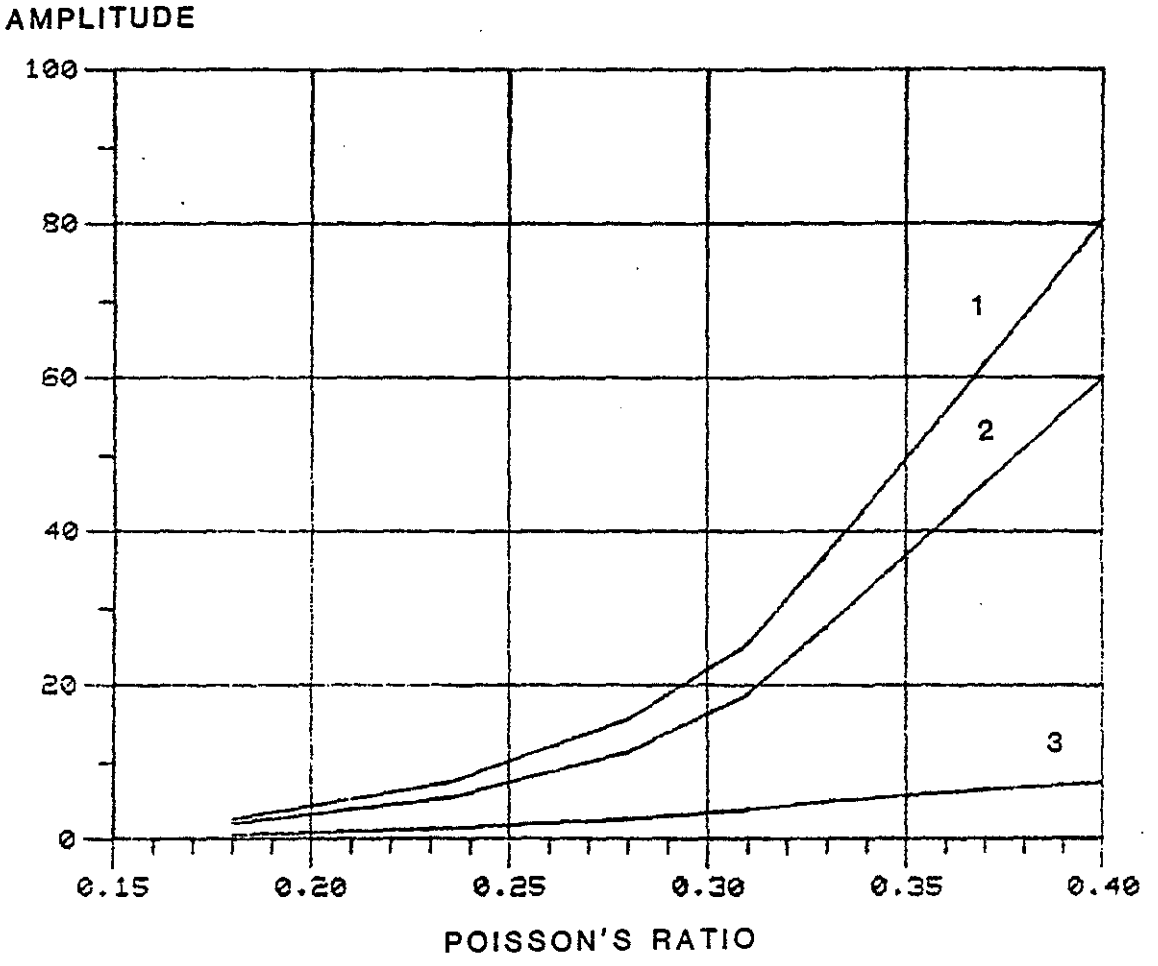

Figure 1: P wave amplitudes versus Poisson's ratio. Curve 1 is for spacing z = 1.5 m, without attenuation; curve 2 is the same as curve 1 with Q_a = 100; curve 3 is the same as curve 1 for z = 10 m.

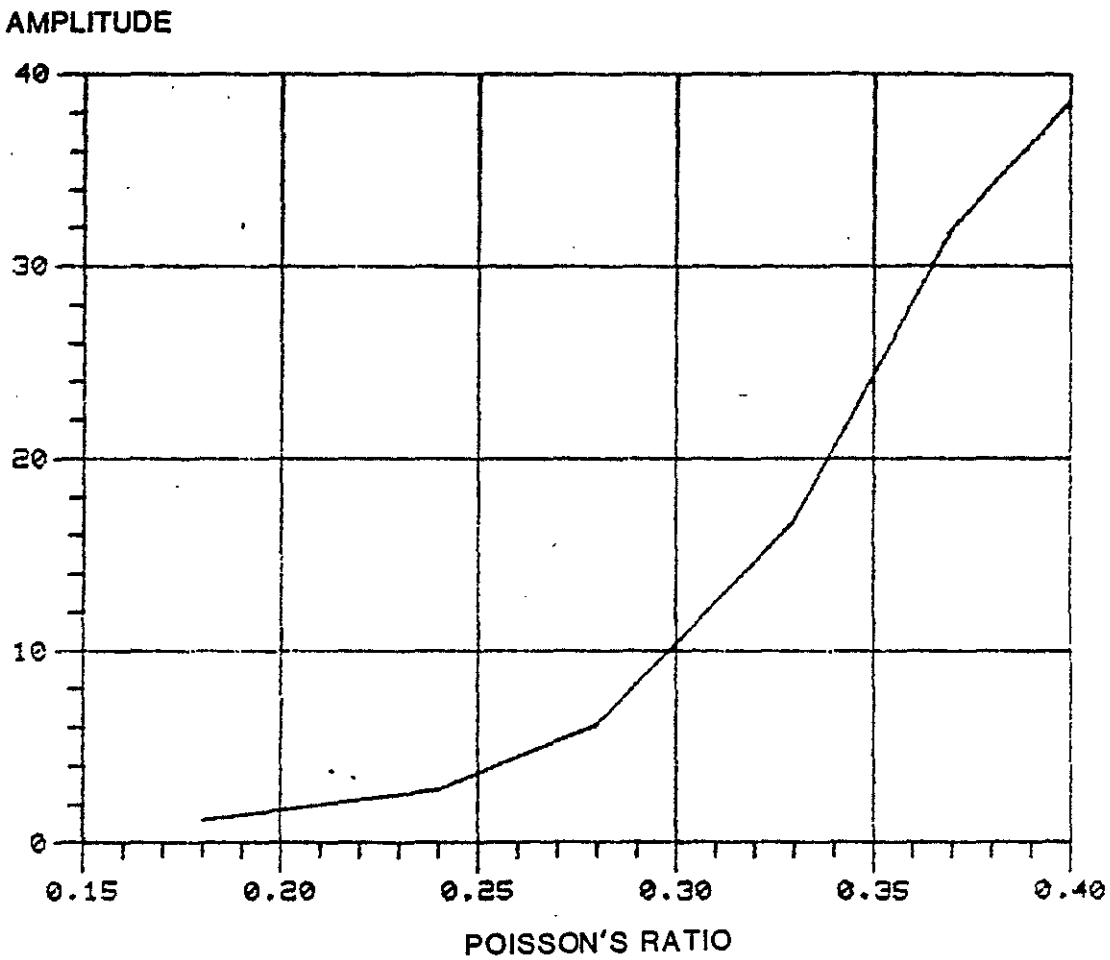

Figure 2: Same as Figure 1 for a formation with a P wave velocity $\alpha = 5.5\ km/s$.

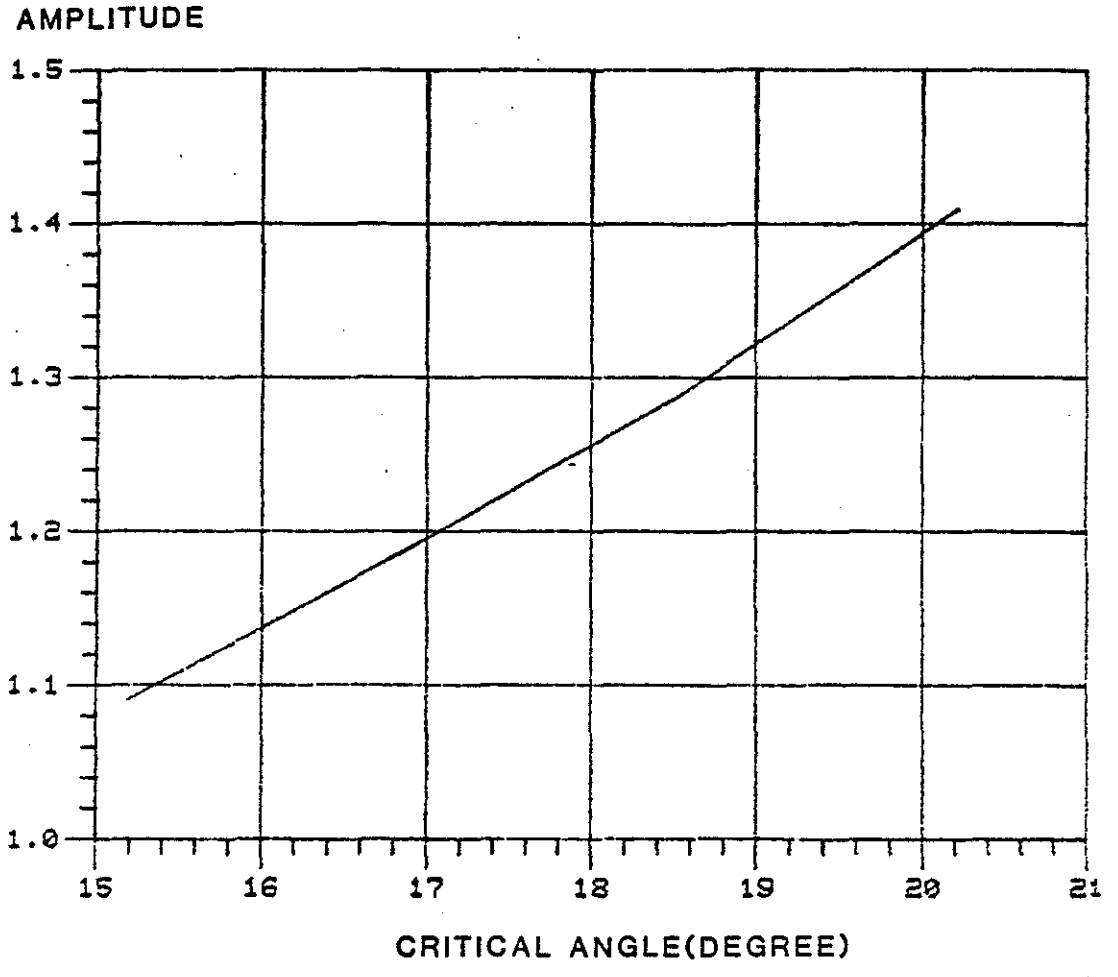

Figure 3: *P* wave amplitude versus critical incident angle.

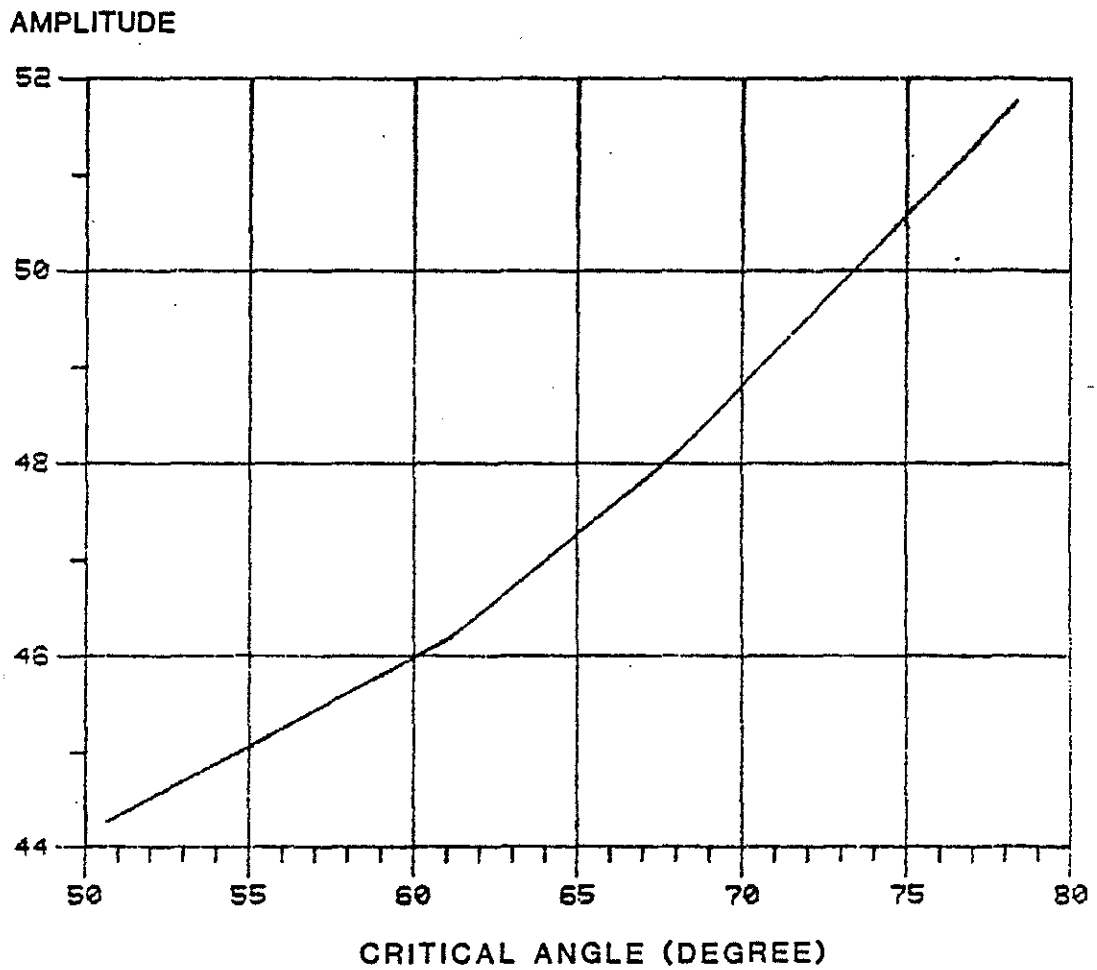

Figure 4: *S* wave amplitude versus critical incident angle.

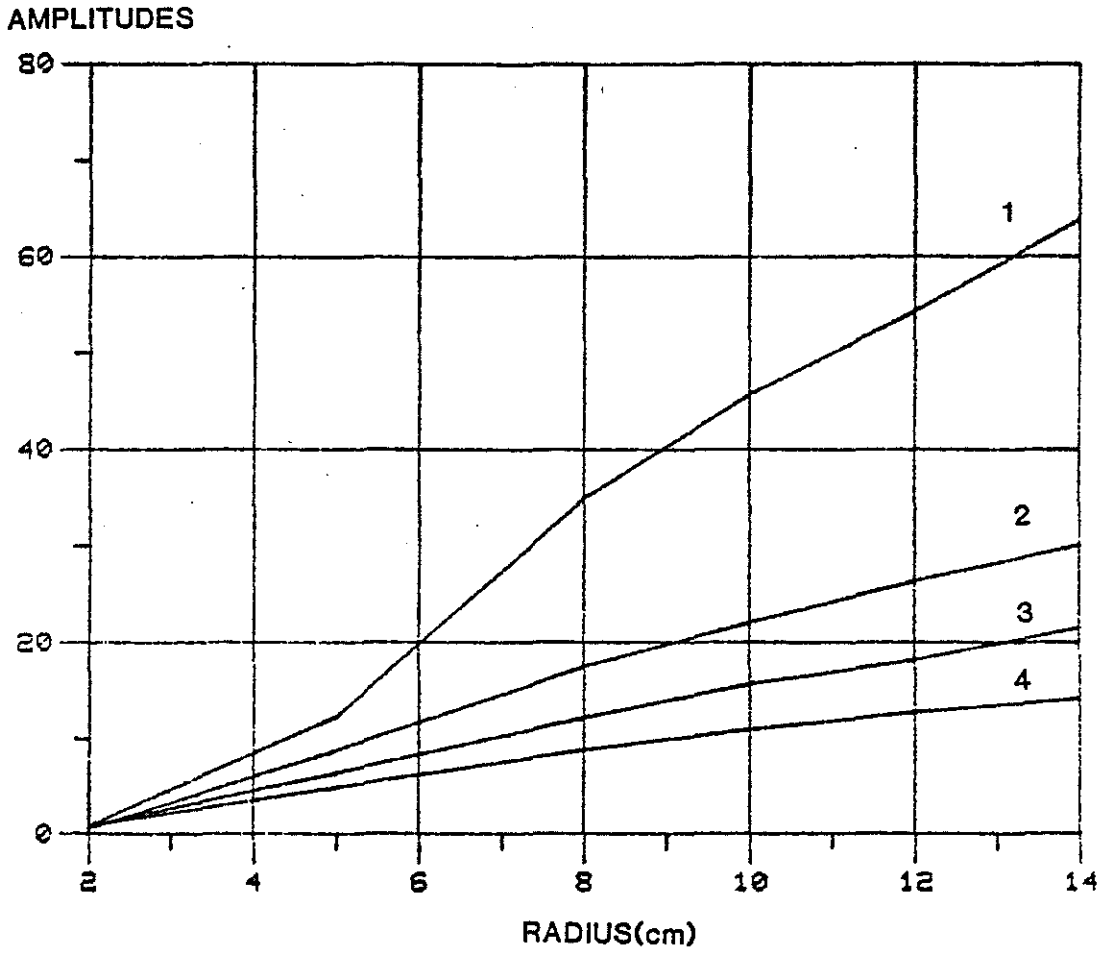

Figure 5: The P and S wave amplitudes as a function of borehole radius with and without attenuation. Curves 1 and 2 are for the S wave, curves 3 and 4 are for the P wave.

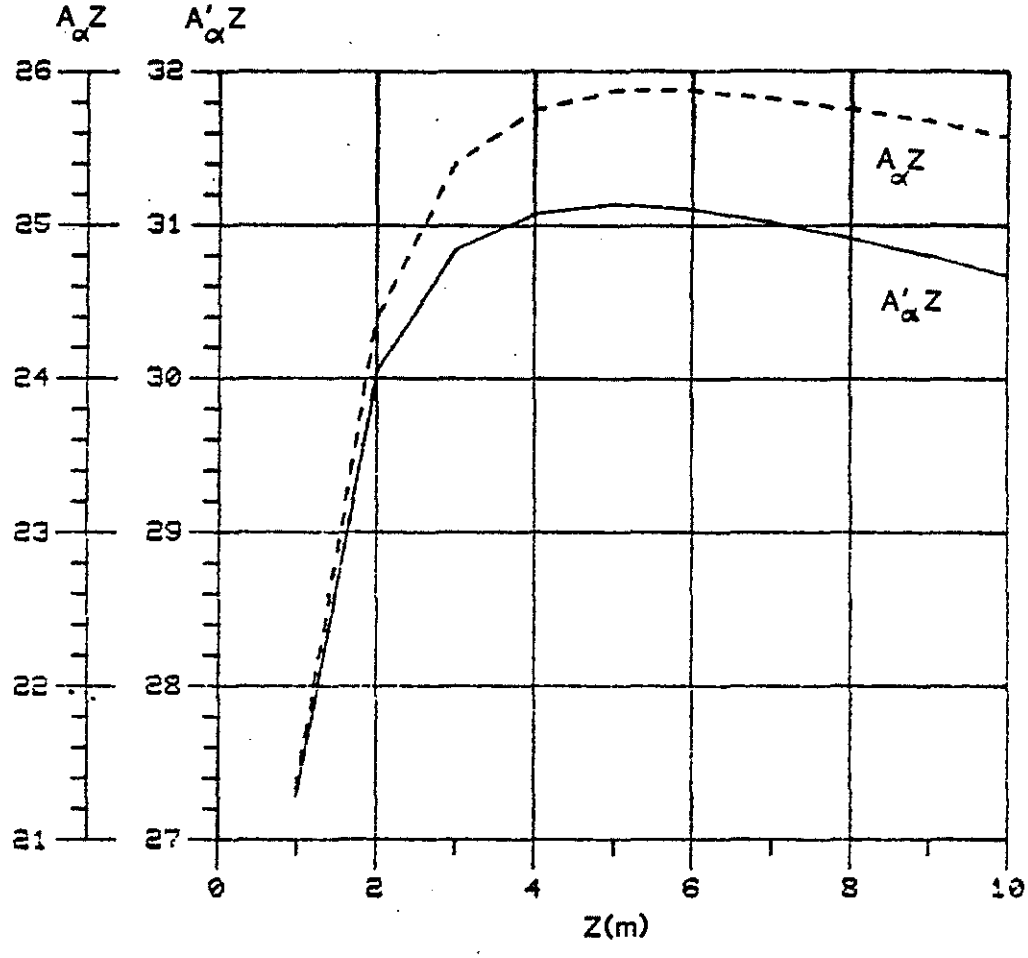

Figure 6: *P* wave amplitude versus source-receiver spacing z.

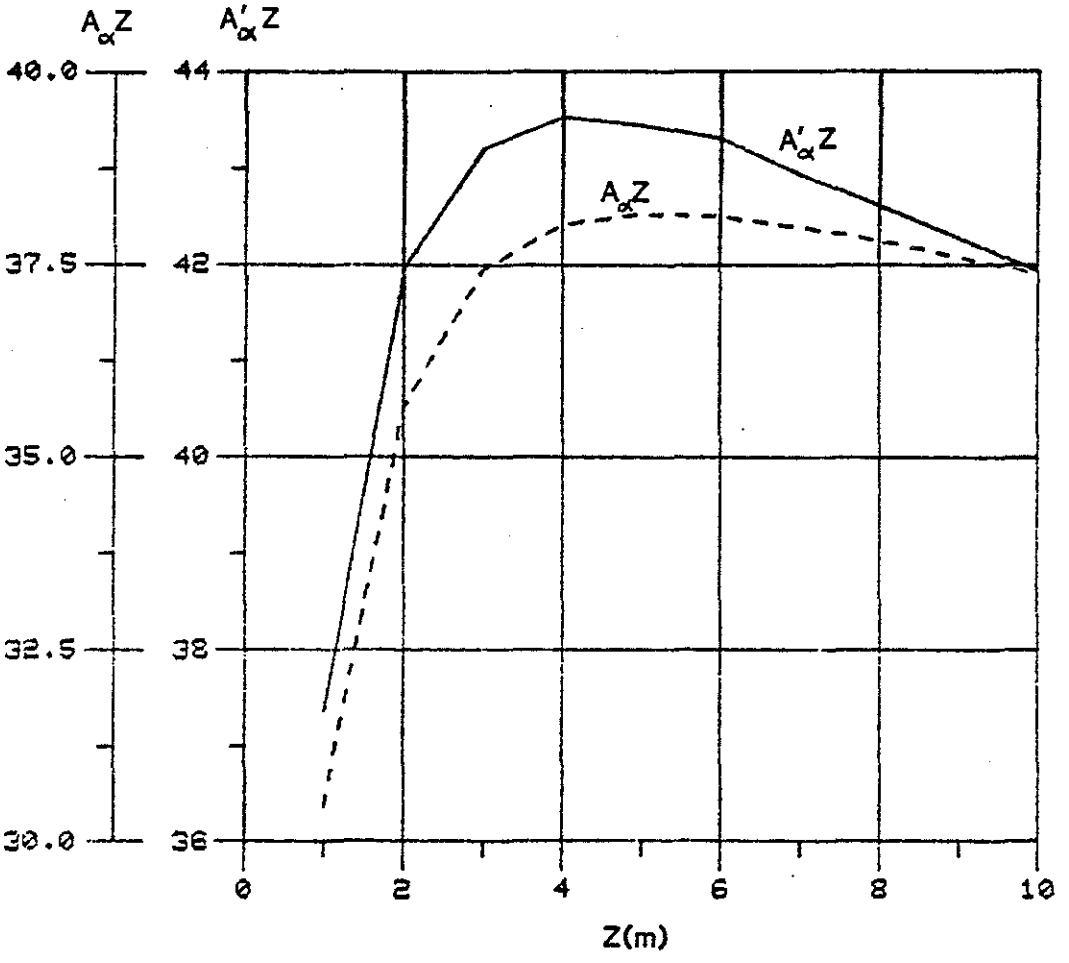

Figure 7: Same as Figure 6 for a radius R = 15 cm.

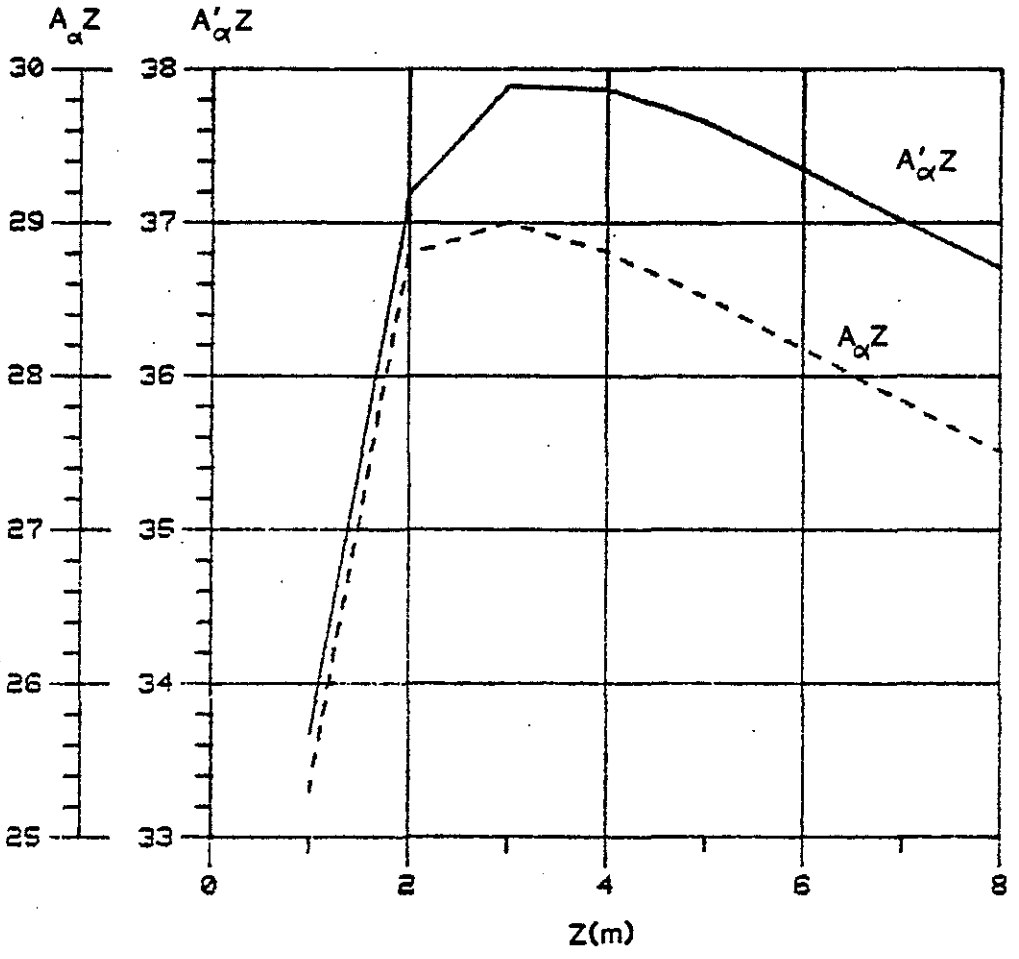

Figure 8: Same as Figure 6 for a frequency $f = 15\ kHz$.

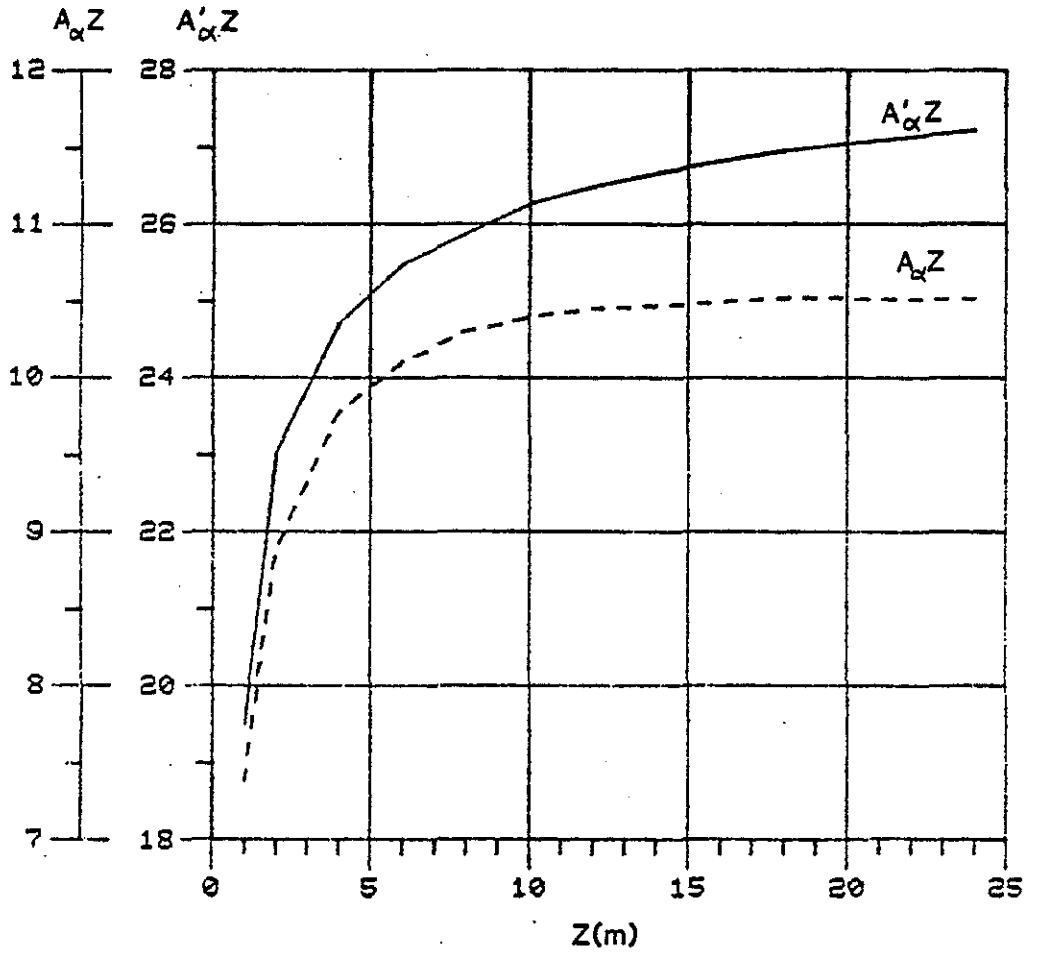

Figure 9: Same as Figure 6 for a frequency $f = 5\ kHz$.

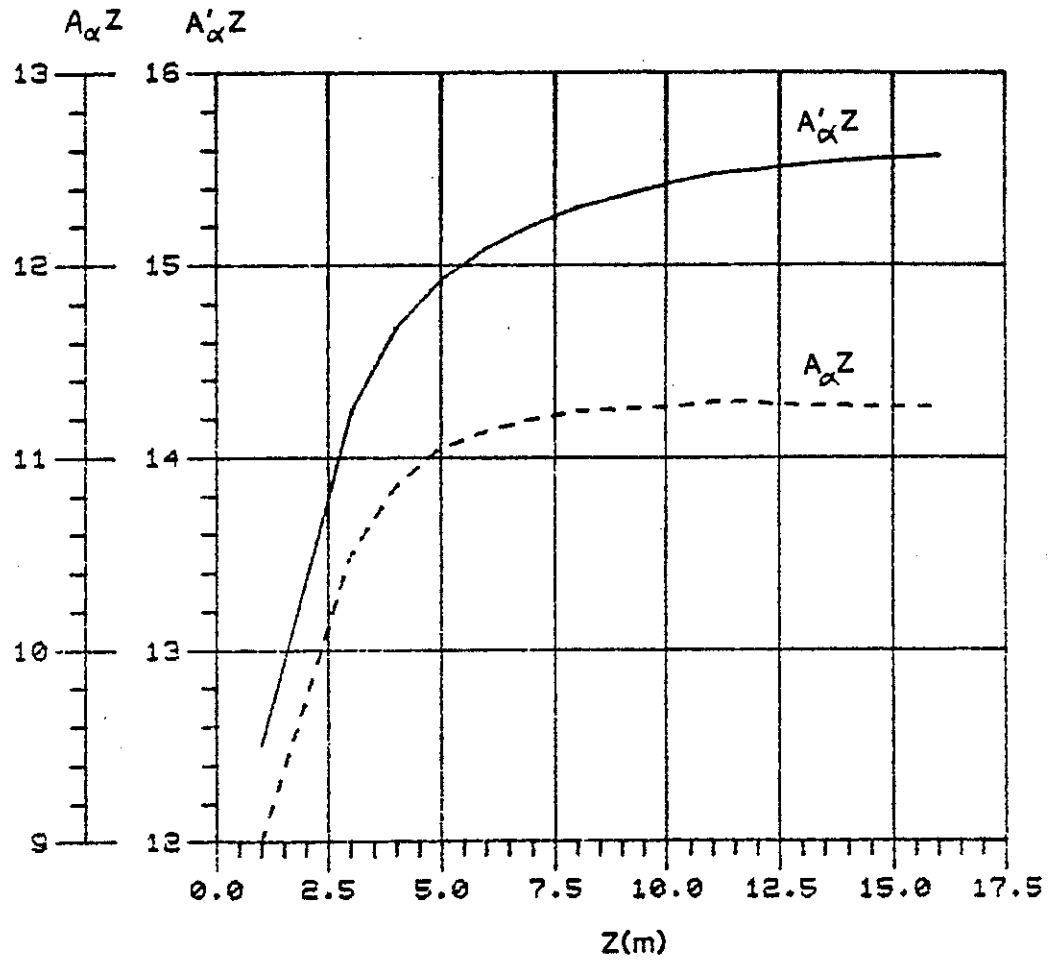

Figure 10: Same as Figure 6 for a formation with α = 5.5 km/s and β = 3.05 km/s.

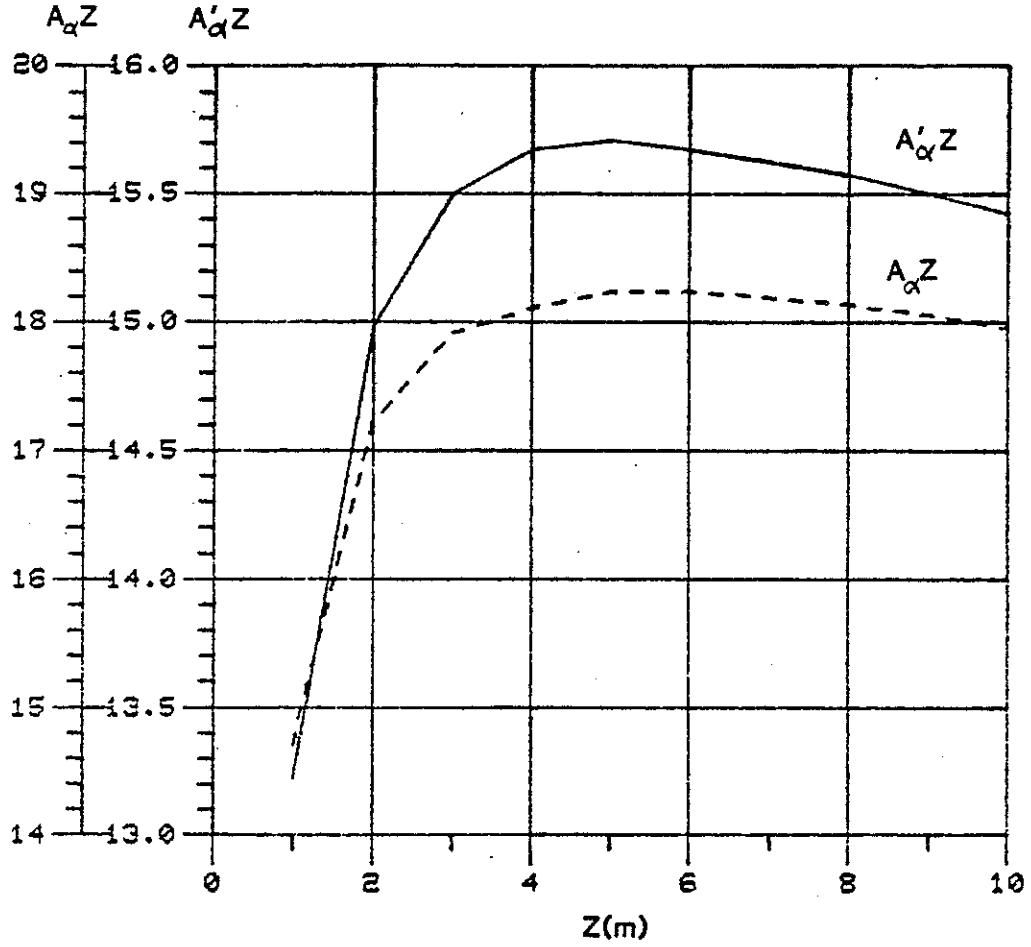

Figure 11: Same as Figure 10 for a frequency f = 15 kHz.

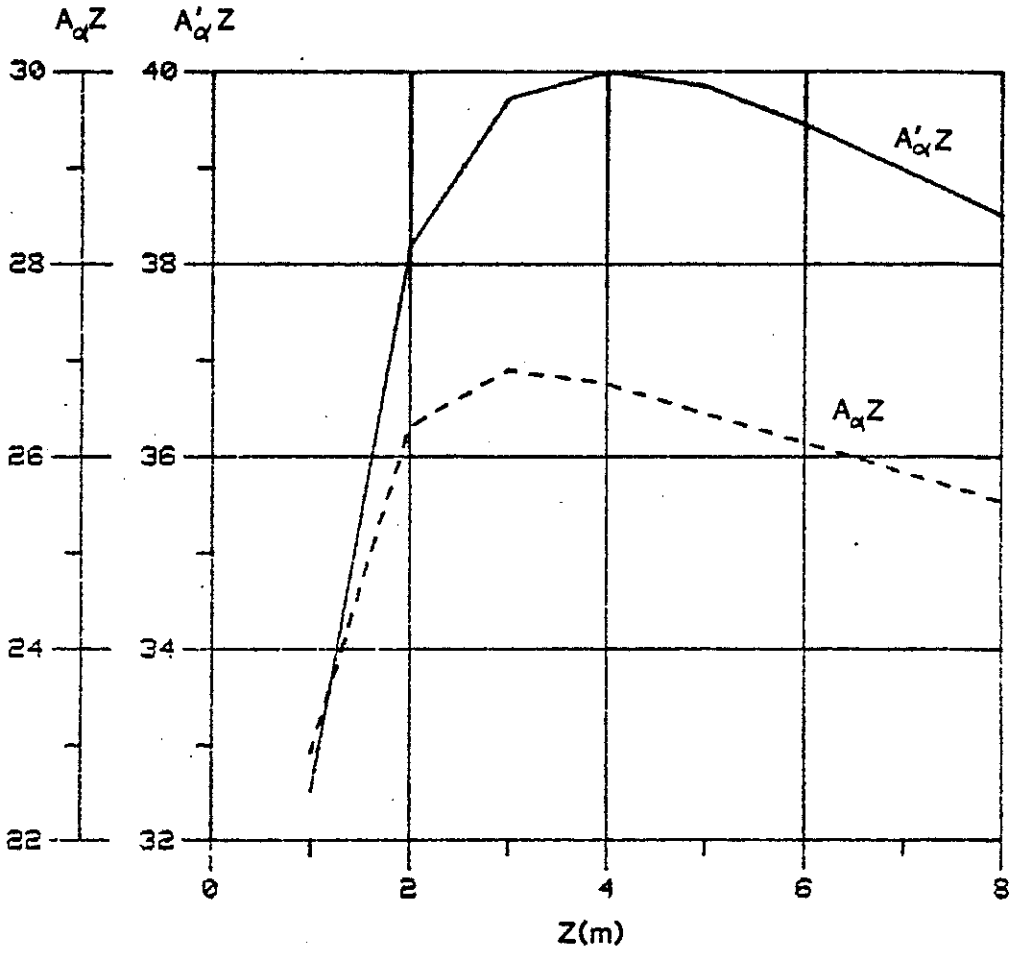

Figure 12: Same as Figure 10 for a Poisson's ratio σ = 0.33. The P wave velocity is held constant.

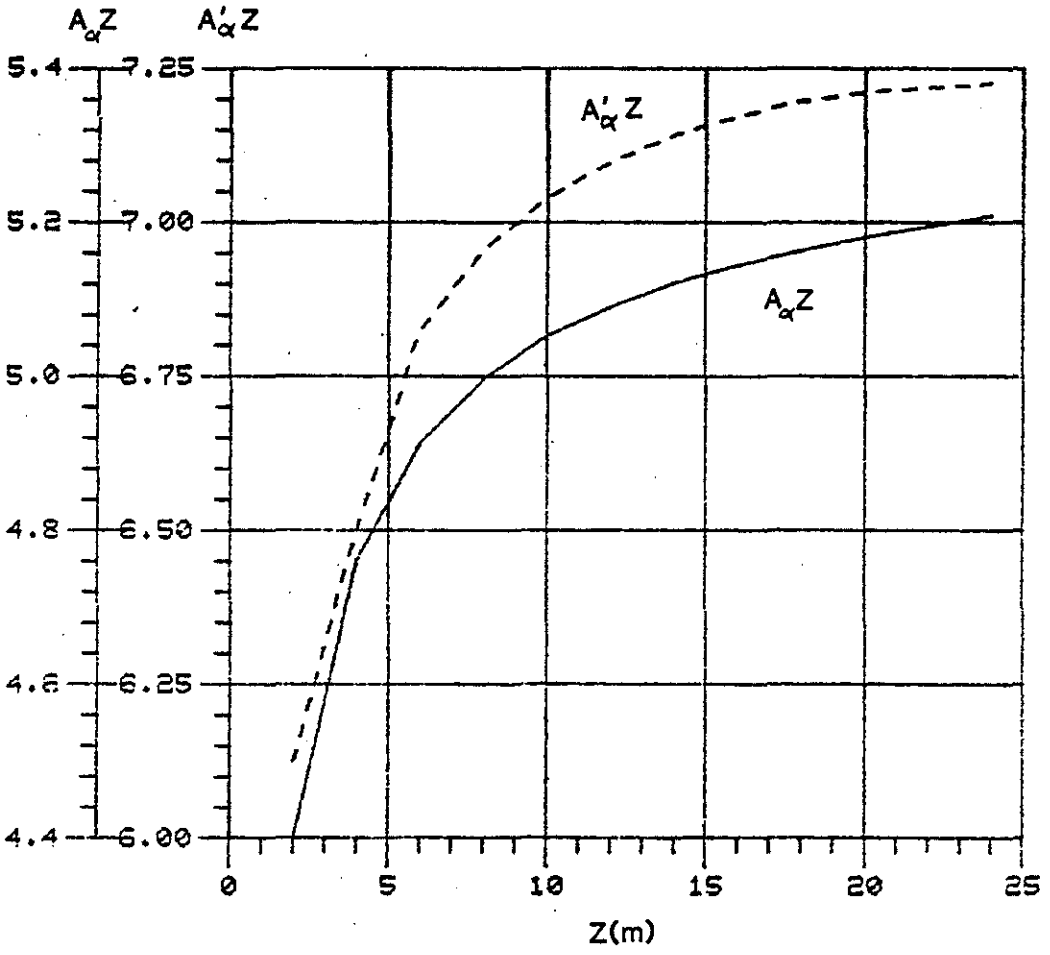

Figure 13: Same as Figure 12 for a Poisson's ratio σ = 0.23.

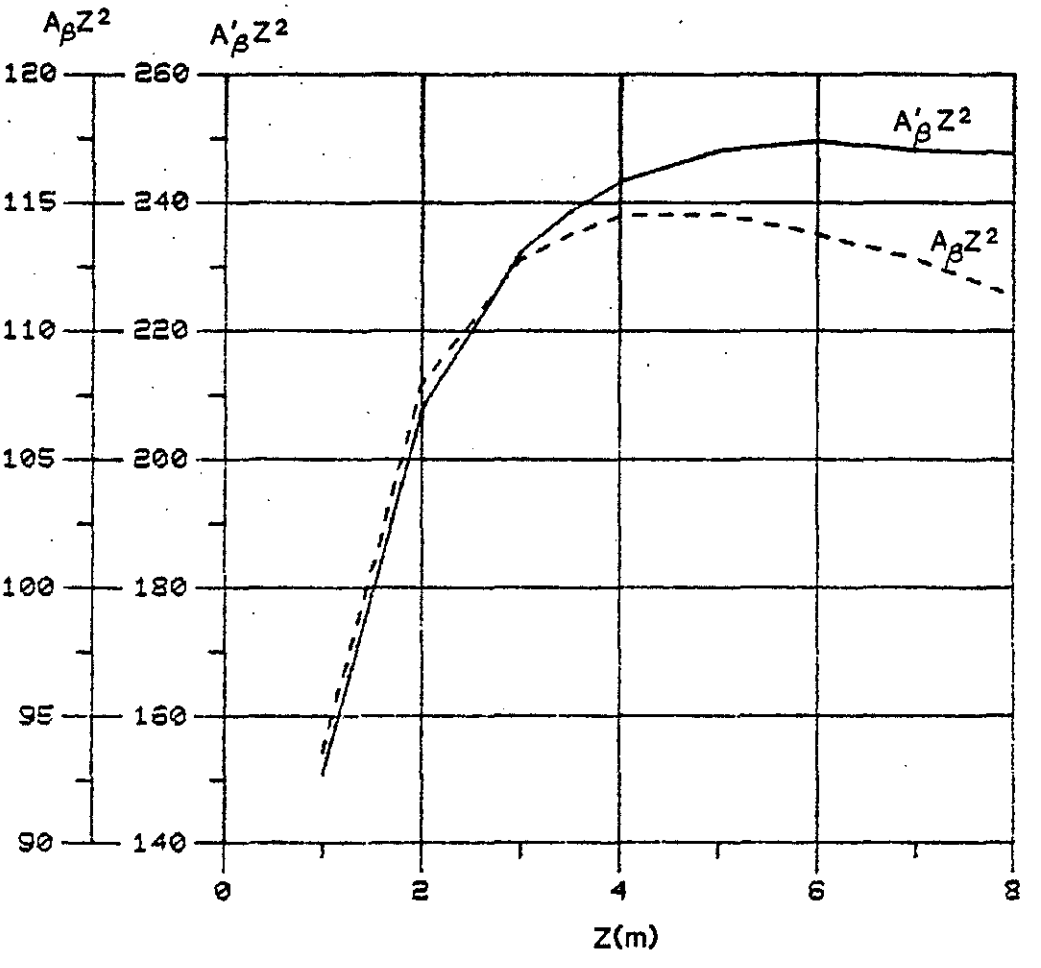

Figure 14: S wave amplitude versus source-receiver spacing z.

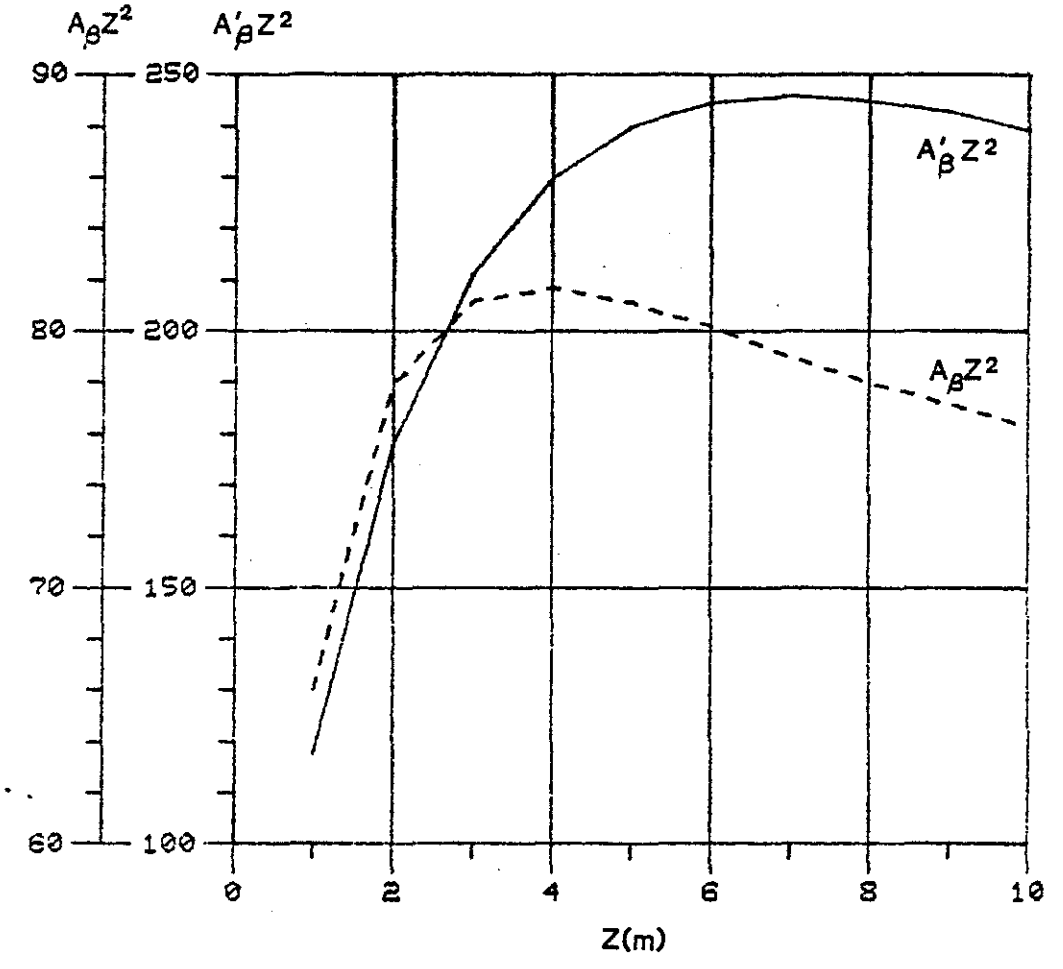

Figure 15: Same as Figure 14 for a radius R = 7.5 cm.

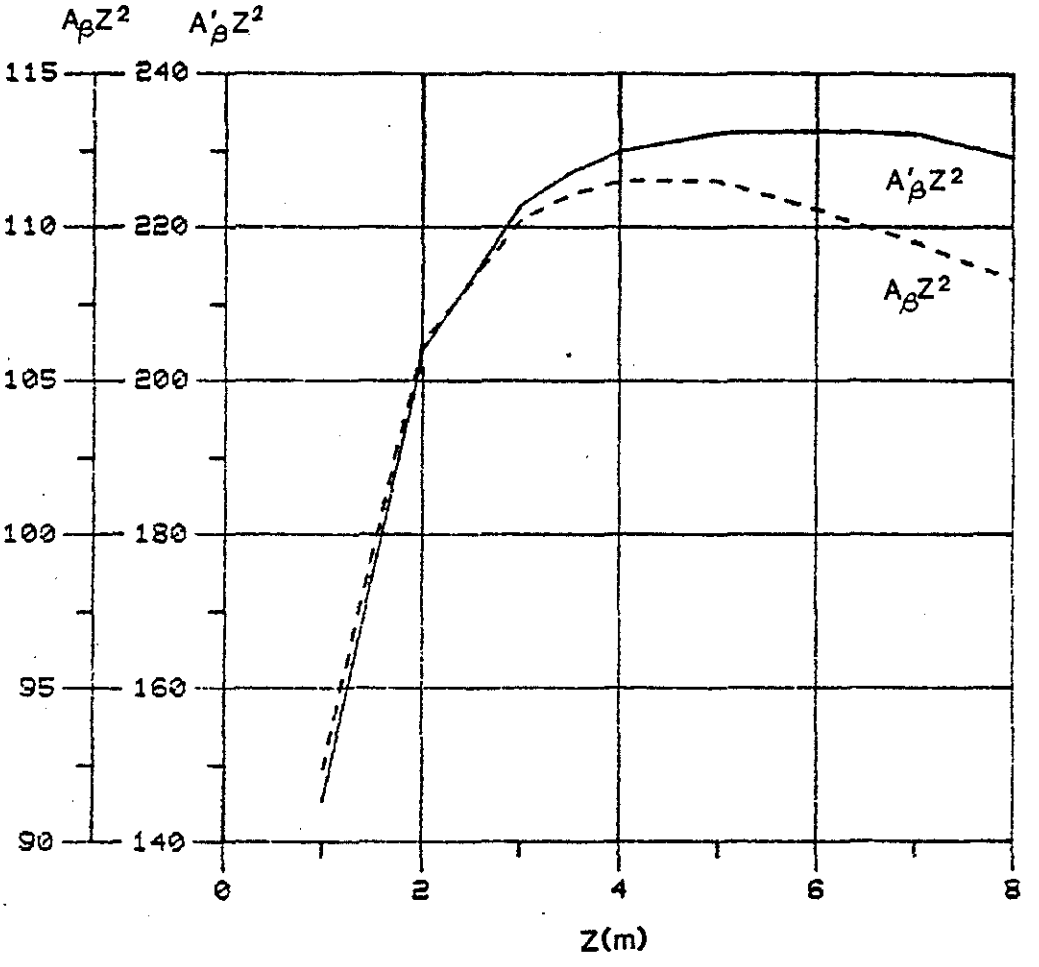

Figure 16: Same as Figure 14 for a Poisson's ratio σ = 0.18. The S wave velocity is held constant.

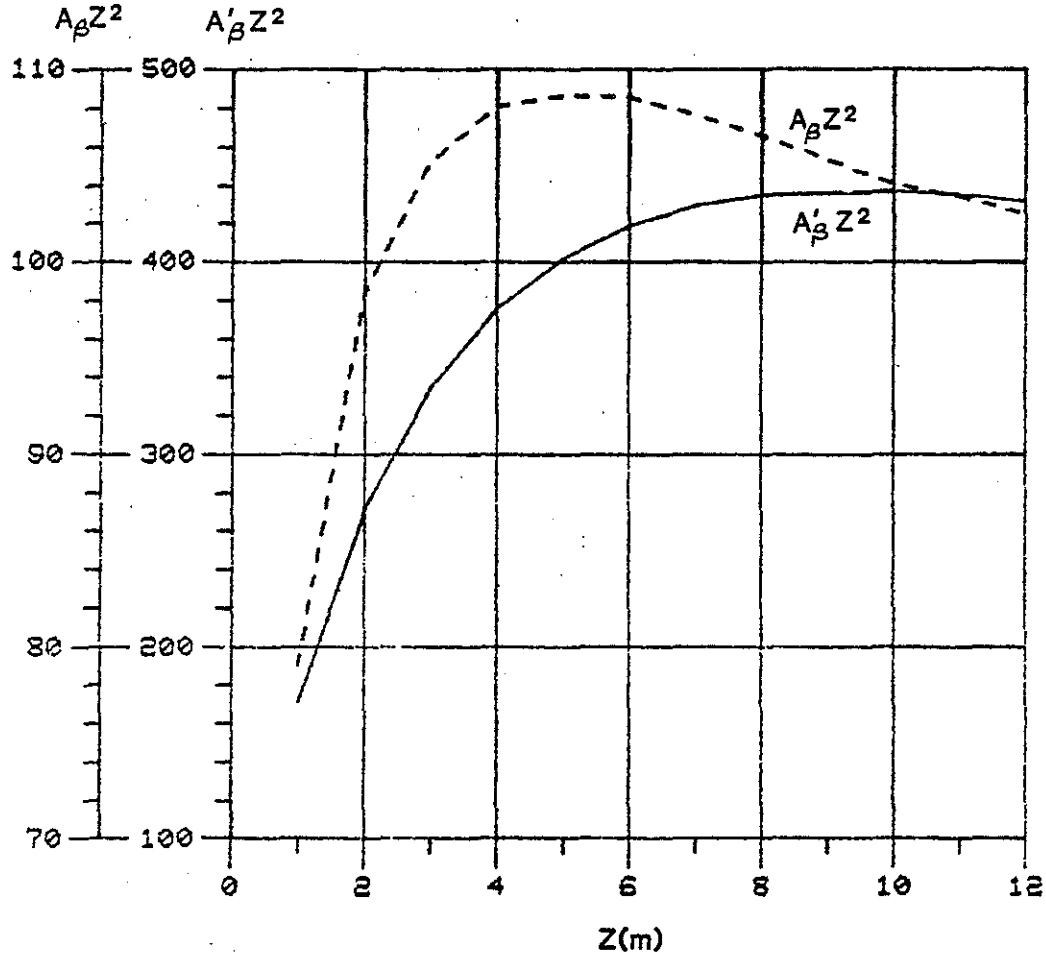

Figure 17: Same as Figure 14 for a frequency f = 7.5 kHz.

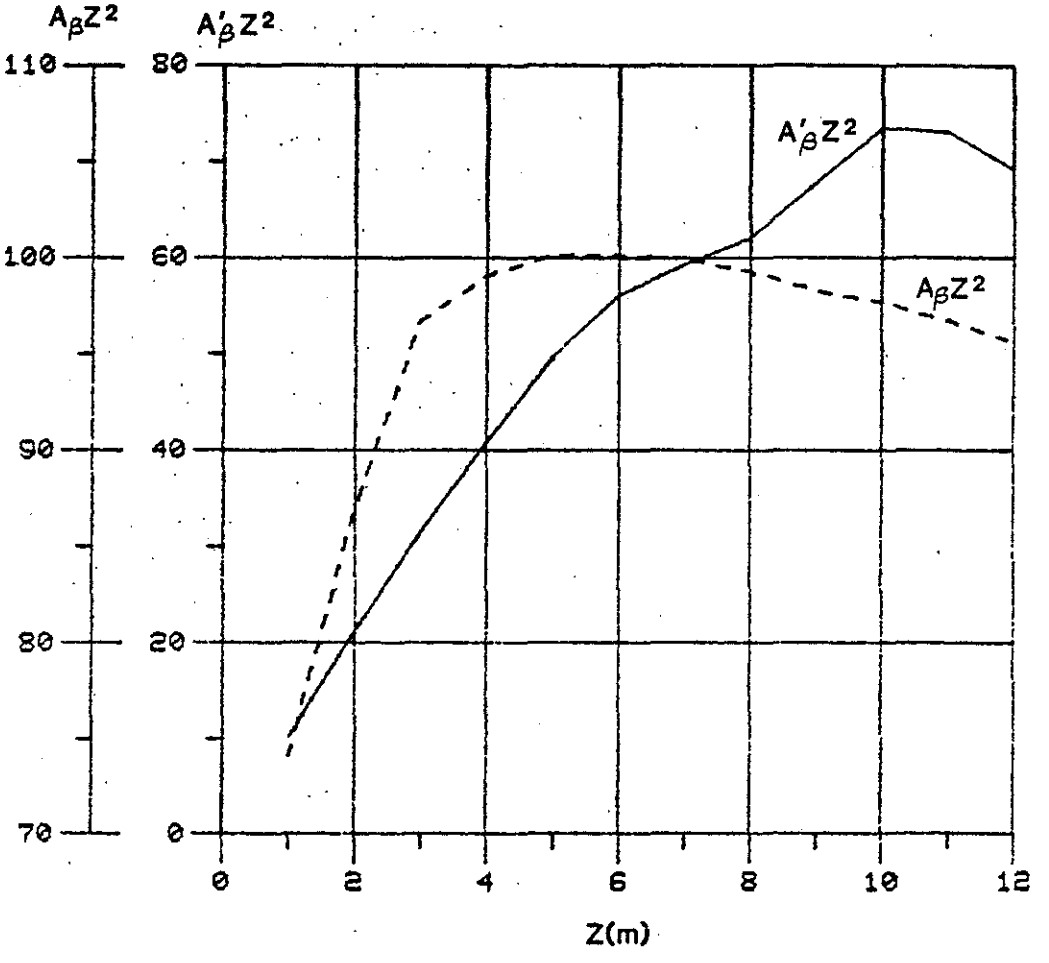

Figure 18: Same as Figure 14 for a formation with α = 5.5 km/s and β = 3.05 km/s.

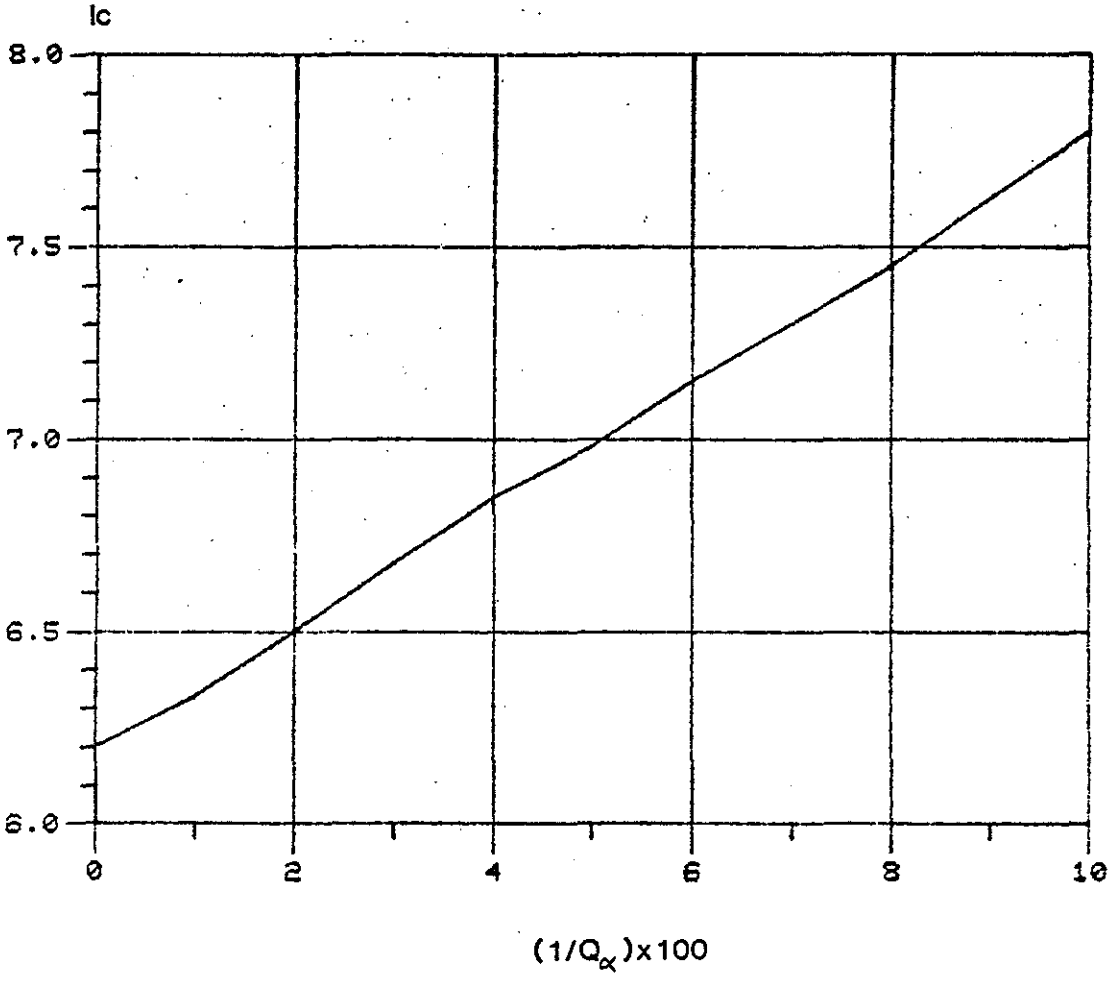

Figure 19: Index of P wave shape I_c versus *in situ* attenuation ($1/Q_\alpha$).